



HAL
open science

Spatial Fluctuations at Vertices of Epithelial Layers: Quantification of Regulation by Rho Pathway

Etienne Fodor, Vishwajeet Mehandia, Jordi Comelles, Raghavan Thiagarajan,
Nir Gov, Paolo Visco, Frédéric van Wijland, Daniel Riveline

► **To cite this version:**

Etienne Fodor, Vishwajeet Mehandia, Jordi Comelles, Raghavan Thiagarajan, Nir Gov, et al.. Spatial Fluctuations at Vertices of Epithelial Layers: Quantification of Regulation by Rho Pathway. *Biophysical Journal*, 2018, 114 (4), pp.939-946. 10.1016/j.bpj.2017.12.026 . hal-02398895

HAL Id: hal-02398895

<https://hal.science/hal-02398895>

Submitted on 22 Dec 2020

HAL is a multi-disciplinary open access archive for the deposit and dissemination of scientific research documents, whether they are published or not. The documents may come from teaching and research institutions in France or abroad, or from public or private research centers.

L'archive ouverte pluridisciplinaire **HAL**, est destinée au dépôt et à la diffusion de documents scientifiques de niveau recherche, publiés ou non, émanant des établissements d'enseignement et de recherche français ou étrangers, des laboratoires publics ou privés.

Spatial Fluctuations at Vertices of Epithelial Layers: Quantification of Regulation by Rho Pathway

É. Fodor,^{1,2,*} V. Mehandia,^{3,4,5,*} J. Comelles,^{3,4} R. Thiagarajan,^{3,4} N. S. Gov⁶
P. Visco,² F. van Wijland,² D. Riveline^{3,4}

¹DAMTP, Centre for Mathematical Sciences, University of Cambridge, Cambridge, United Kingdom; ²Laboratoire Matière et Systèmes UMR 7057 CNRS/P7, Université Paris Diderot, Paris cedex 13, France; ³Laboratory of Cell Physics, ISIS/IGBMC, Université de Strasbourg and CNRS (UMR 7006), Strasbourg, France; ⁴Development and Stem Cells Program, IGBMC, CNRS (UMR 7104), INSERM (U964), Université de Strasbourg, Illkirch, France; ⁵School of Mechanical, Materials and Energy Engineering, Indian Institute of Technology, Ropar, India; and ⁶Department of Chemical Physics, Weizmann Institute of Science, Rehovot, Israel

Abstract

In living matter, shape fluctuations induced by acto-myosin are usually studied *in vitro* via reconstituted gels, whose properties are controlled by changing the concentrations of actin, myosin and cross-linkers. Such an approach deliberately avoids to consider the complexity of biochemical signaling inherent to living systems. Acto-myosin activity inside living cells is mainly regulated by the Rho signaling pathway which is composed of multiple layers of coupled activators and inhibitors. We investigate how such a pathway controls the dynamics of confluent epithelial tissues by tracking the displacements of the junction points between cells. Using a phenomenological model to analyze the vertex fluctuations, we rationalize the effects of different Rho signaling targets on the emergent tissue activity by quantifying the effective diffusion coefficient, the persistence time and persistence length of the fluctuations. Our results reveal an unanticipated correlation between layers of activation/inhibition and spatial fluctuations within tissues. Overall, this work connects the regulation via biochemical signaling with mesoscopic spatial fluctuations, with potential application to the study of structural rearrangements in epithelial tissues.

*These authors contributed equally to this work.

INTRODUCTION

Changes in shapes of cells and tissues are mediated by the acto-myosin cytoskeleton. To reproduce the dynamics of this network, minimal systems made of actin filaments, myosin motors and cross-linkers are synthesized *in vitro* (1–5). The mechanics and dynamics of such *active gels* are controlled by varying the concentration of their various components. Activity of each component is monitored by adding some inhibitor drugs, and/or by tuning the ATP concentration of the system. Recent experimental evidence have shown the relevance of this approach to investigate the role of motors and cross-linkers in the emerging properties of the network (2, 6). These studies are based on tracking the motion of tracers injected in active gels: analyzing the spontaneous fluctuations of such tracers enables one to extract information about the activity of internal motors.

In multicellular systems, such as tissues of developing embryos, acto-myosin drives the *morphogenesis*: dramatic rearrangements leading to the formation of distinct

organs (7, 8). This remodelling is mainly under the control of intracellular activity, which powers spatial fluctuations (9), and intercellular interactions mediated by adhesion between neighboring cells (10, 11). In contrast to synthetic gels, the internal regulation of the cellular acto-myosin activity is more complex *in vivo*. Therefore, extending the *in vitro* approach, based on controlling externally the activity of each specific component, to *in vivo* situations requires new strategies.

The Rho signaling pathway is known to regulate the acto-myosin activity in living cells (12). It also controls cell-cell junctions (13) and the elasticity of stress fibers (14). Such a pathway can be viewed as a series of activators and inhibitors installing a hierarchy of potential targets (15, 16). Activations and inhibitions controlled by each target are such that anticipating their net effects on the tissue fluctuations, powered by acto-myosin activity, remains a challenge (17, 18). In that respect, the inherent complexity of internal activity *in vivo* calls for new experiments and quantitative analysis

to bridge the biochemical signaling of the Rho pathway with the emerging tissue dynamics.

In this paper, we explore the regulation of active fluctuations by the Rho pathway in epithelial monolayers. We measure these fluctuations by tracking tricellular junctions or vertices over time. In contrast with active gels, our analysis of internal fluctuations does not require to inject external tracers. Based on a phenomenological model, we quantify key parameters of junction activity: their effective diffusion coefficient, as well as the persistence time and persistence length of spatial fluctuations. We report modifications of these parameters for various targets along the signaling pathway. These results support that, for the inhibitions that we considered, the active fluctuations of the vertices are reduced when going downstream in the Rho pathway inhibition.

MATERIALS AND METHODS

Experiments were performed with MDCK II cells stably expressing E-cadherin GFP (Nelson Lab.). We culture cells in DMEM containing 10% Fetal Calf Serum (FCS) and antibiotics. We replate them on glass coverslips (CS) of 25 mm diameter for live cell imaging. When the cell monolayer covered 70% of the CS area, we firmly place the sample at the bottom of a custom made metallic holder. For acquisition, we change the medium to L15, 10% FCS and antibiotics. We use the following inhibitors from myosin up to Rho at optimal concentrations following the manufacturer recommendations: inhibition of acto-myosin by ML-7 (Sigma-Aldrich, 10 μM), inhibition of Rho kinase (ROCK) by Y-27632 (Sigma-Aldrich, 10 μM), and inhibition of Rho by C3 Transferase (Cytoskeleton, 0.04 μM). Note that the use of blebbistatin to inhibit directly myosins yielded some detrimental effects, leading us to rather use ML-7 instead.

For observation, we use a motorized inverted microscope (Nikon Eclipse Ti), equipped with a 12 bit CCD camera (Photometric CoolSNAP HQ2). The setup is temperature controlled at 37°C (Life Imaging Services). We check with fluorescent beads (4 μm , TetraSpeck, Invitrogen Molecular Probes) grafted on CS surface that no drift appears during 24 hours of live imaging after 2 hour stabilization. We take pictures of the monolayer every 5 min during the next 8 hours with multiple z-stacks 1 μm apart. They span 3 μm depth of the cell monolayer. We merge the z-stacks into one image by using the maximum intensity projection. We then extract vertex positions from the sequence of merged images by manually clicking in each frame as long as they are visible. The procedure was validated in its precision through automatized detection as well. For each condition, we check that the average cell area was always about $180 \pm 15 \mu\text{m}^2$, and we consider more than 20 vertices for at least 3 biological repeats.

RESULTS

Vertex tracking and inhibitors in the Rho pathway

We use Madin Darby Canine Kidney (MDCK) cells stably transfected with E-cadherin fused with the Green Fluorescent Protein (GFP) as a paradigm for epithelial tissues dynamics (19). This allows us to study live cells while interacting with each other. We seek to identify spatial points primarily involved in tissue transformations. The meeting points between three cells are involved in exchanges between neighbouring cells, thus serving as hallmark of tissue dynamics (11, 20). Some specific proteins, such as tricellulin, are known to accumulate at this point in cell culture. Besides, vertices have also attracted the attention of developmental biologists which exhibit accumulation of proteins at these specific points (21).

Vertex dynamics are driven both by thermal fluctuations and by active fluctuations powered by some internal nonequilibrium processes such as motor-induced forces, actin polymerization and cell-cell adhesion. The myosin-II motors are localized in dense contractile units present in the apical surface of the tissue (22, 23) [Figs. 1(a-c)]. The active forces lead to large displacements of the vertices distinct from the thermal fluctuations of smaller amplitude. We focus here on large displacements which do not lead to any topological transitions in the tissue [Figs. 1(d-e)]. The Rho signaling pathway controls the acto-myosin activity inside cells, namely the forces induced by myosin and/or by actin polymerization (see Fig. 9 in (16)). In this study, we focus on the downstream targets that affect myosin to establish the principles for the validity and relevance of our framework. Upstream and downstream targets install a hierarchy in the activation of myosin. We specifically inhibit the following targets: Rho, Rho kinase (ROCK) and myosin-II [Fig. 1(f)]. Each inhibitor is specific to its target and incubated at the optimal concentrations for its inhibition. We used standard concentration values already utilized in other cell biology studies for many cell types including MDCK (24–27). Altogether, we probe four conditions on the same system by considering untreated cells as a control.

To demonstrate that the chosen inhibitors and their concentration specifically act on the contractile state of cells, we investigate their effect on both architecture and contractile forces within tissues by measuring single cell area and myosin cluster area in each condition. The distribution of single cell area is not strongly affected in the myosin-II inhibitor case compared with control, as apparent from the mean value in Fig. 1(g). The distribution gets modified in the Rho kinase and Rho inhibitor cases, with mean values being slightly reduced and increased, respectively. In contrast, the polygonicity distribution remains approximately the same for all conditions at different times, supporting that tissue architecture is barely affected by external inhibitors (see Fig. S1 in the Supporting Material).

Myosin clusters have been shown to be relevant read-outs to assess the contractile state of cells (28, 29). Along this line, measurements of cluster characteristics are informative. In our case, the mean density value of myosin clusters for control is larger than in the inhibited cases (see

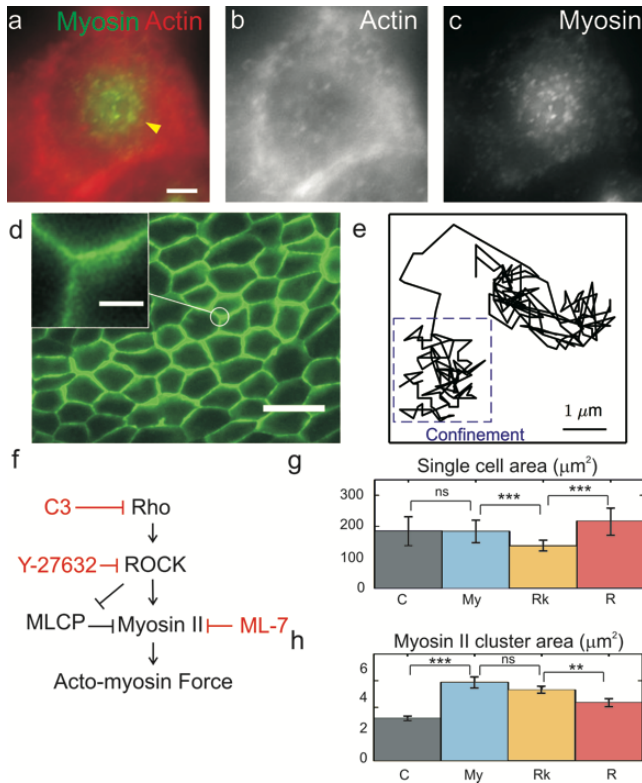


Figure 1: Study of vertex fluctuations. (a) Actin (red) and myosin (green) structures at the apical surface of a MDCK cell (scale bar $3 \mu\text{m}$). The myosin is concentrated in dense contractile units (yellow arrow) referred to as myosin clusters. (b) Actin structure alone. (c) Myosin structure alone. (d) We visualise MDCK cell monolayer by GFP E-cadherin (scale bar $30 \mu\text{m}$). (Inset) We identify the meeting points between three cells as the privileged point for our analysis (scale bar $4 \mu\text{m}$). (e) Extraction of a typical transition between two locally stable positions in vertex trajectory (total time 8 hours). (f) Simplified diagram of the Rho pathway installing an order relation in myosin activation, as presented in (16); in red the specific inhibitors and their targets. (g) Area of individual cells in each condition. C: Control; My: Myosin inhibitor; Rk: Rho kinase (ROCK) inhibitor; R: Rho inhibitor. Number of experiments \times number of cells = C: 4×235 ; My: 4×246 ; Rk: 3×249 ; R: 3×148 . (h) Area of myosin clusters. Number of experiments \times number of clusters = C: 2×312 ; My: 2×186 ; Rk: 2×197 ; R: 2×257 . Statistical analysis with one-way ANOVA test: ns (non significant) $p > 0.05$, * $p < 0.05$, ** $p < 0.01$, *** $p < 0.001$ (see the Supporting Material).

Fig. S2 in the Supporting Material), suggesting a decrease in force generation for the same level of myosin per cell. In addition, the area of each myosin cluster is smaller in control than in other conditions [Fig. 1(h)]. Besides, this area increases the more downstream along the Rho pathway inhibition, suggesting a relaxation of the myosin pool in the apical side, consistently with the notion that myosin-induced forces are reduced. Altogether, our analysis of clusters confirms that we are acting on the contractile state of cells. Since inhibitors are specific and used at their optimal concentrations, these measurements support the validity of our experimental approach.

Statistics of vertex displacement: inhibitors affect spatial fluctuations

Our goal is to investigate how the emergent fluctuations of the tissue are regulated by the Rho pathway. To this aim, we first demonstrate that the inhibitors in the pathway affect these fluctuations by extracting the statistics of displacements from the vertex trajectories. This allows us to assess the existence of a direct link between biochemical signaling and mechanical fluctuations. In our analysis, we do not consider neither spatial inhomogeneities nor topological transitions that occur in the tissues. In that respect, we measure vertex trajectories in the absence of neighboring cell division, by tracking them as long as they are visible until a maximum of 8 hours.

We compute the projected one-dimensional mean square displacement (MSD) within the four different conditions [Fig. 2(a)]. For each condition, the short time MSD exhibits a power-law behavior with exponent close to 0.7 over about one decade. Interestingly, a subdiffusive behavior was reported for the dynamics of vertices in the endoplasmic reticulum (30). The large time MSD depends on conditions and exhibits a behavior that, for simplicity, we have characterized by a power-law. The corresponding exponent is typically larger than 1, except for myosin inhibitor where it is smaller. The crossover between the two regimes appears between 20 and 60 min. Fluctuations are reduced in the myosin inhibited case, which has the lowest MSD, and they are enhanced for the Rho inhibitor, where the long time MSD is the largest. We also explore the full statistics of vertex displacement by measuring the probability distribution function (PDF) for each condition, as shown in Figs. 2(b-e). At short time the PDF is Gaussian, while it exhibits broader tails at large time. These tails reveal large displacements of the vertex, and were already observed for tracer particles in active gels (31) and living cells (32–36). They are more pronounced in the Rho inhibitor case, as a signature of larger fluctuations, possibly due to directed motion events.

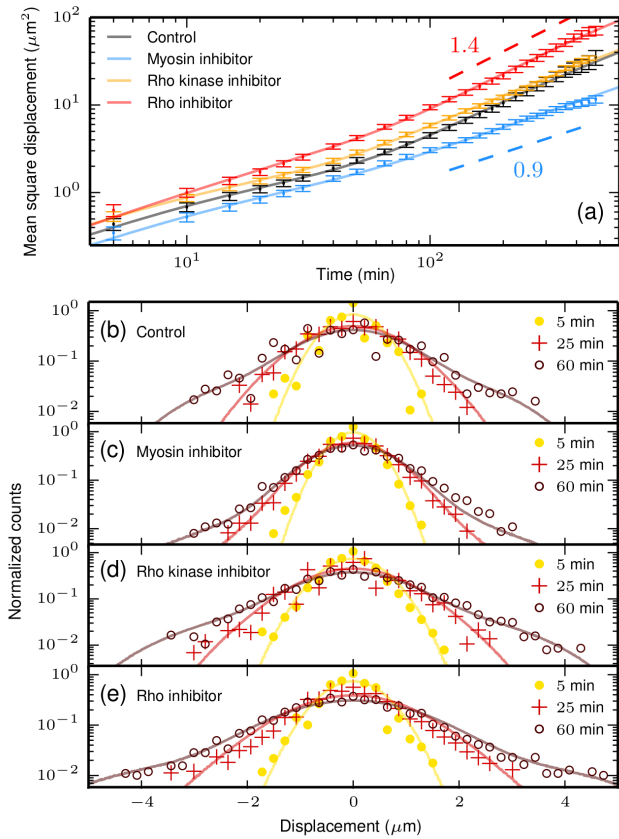


Figure 2: Statistics of vertex displacement. (a) Mean square displacement as a function of time in four conditions: control (black), myosin inhibitor (blue), Rho kinase inhibitor (orange), and Rho inhibitor (red). The corresponding best fitting curves are in solid lines. The blue and red dashed lines report the large time behaviors. (b-e) Distribution of displacement for the four conditions at three times: 5 min (●), 25 min (+), and 60 min (○). Exponential tails appear at long times as a consequence of directed motion events in vertex dynamics. Results of simulated dynamics are in solid lines.

Phenomenological model of vertex dynamics: transient confinements and large displacements

To quantitatively discriminate between the effects of the different inhibitors, we analyze our measurements with a nonequilibrium model previously introduced to describe tracer fluctuations inside living cells (36). This model is not aimed at describing any specific process that produces the active fluctuations, it rather formulates a general framework that allows one to quantify non-equilibrium forces and fluctuations. We regard the vertex as a virtual particle which dynamics is prescribed by two coupled equations: (i) an equilibrium diffusion of the vertex in a cage, modelled as an harmonic potential of stiffness k —the displacement is driven by a Gaussian white noise of variance $2\gamma k_B T$ with a drag force of coefficient γ ; (ii) a non-Gaussian colored diffusion

equation for the center of the cage, mimicking nonequilibrium activity as a run-and-tumble dynamics. Inspired by the large ballistic-like displacements that we observe in experimental trajectories, we model this active noise as a two-state Poisson process: the cage has a constant velocity v in a random uniformly sampled two-dimensional direction during a random persistence time of average τ , and it remains fixed during a random quiescence time of mean τ_0 . We understand the confinement as an elastic mechanical stress resulting from cells surrounding each vertex, and the nonequilibrium motion of the cage as an active stress. The effect of this active stress is to reorganize the structure of the monolayer, and therefore to spatially redistribute the elastic mechanical stress.

In the absence of activity, this model predicts a short time diffusion, and then a large time plateau expressing the elastic confinement. Such dynamics is entirely under the control of equilibrium thermal fluctuations. In an active system, nonequilibrium processes enhance vertex displacement *via* the cage motion, yielding a free diffusion of the vertex with coefficient $D_A = (v\tau)^2/[2(\tau + \tau_0)]$. The large time dynamics is fully determined by the active parameters $\{v, \tau, \tau_0\}$, whereas thermal fluctuations control the short times *via* $\{k, \gamma, T\}$. A sub-diffusive transient regime appears between the two diffusions, as a crossover towards a plateau, and a super-diffusive regime can also precede the large time diffusion, as a signature of the ballistic motion involved in the active noise. In such a case, thermal effects are negligible at times larger than $\tau_c = \sqrt{\tau k_B T / (k D_A)}$, a timescale quantifying the transition from the short time equilibrium-like dynamics to the large time active diffusion. Simulated trajectories exhibit clusters of similar size accounting for the transient confinement of the vertex. Occasionally large displacements of order $v\tau$ appear. The vertices do not only fluctuate around a local equilibrium position, they also undergo rapid directed jumps (compare Fig. 1(e) and Fig. 3(a)).

In contrast to previous works which describe the many-body dynamics of cells in the tissue in a more complete framework (37–39), we do not explicitly account for interactions between neighbouring vertices. As a result of such interactions, the cells experience an intermittent dynamics alternating between fluctuations of small amplitude and rapid large displacements. As in glassy systems, the jumps appear through collective rearranging regions (40), thus contributing to the non-Gaussian fluctuations experienced by the vertices. Even though non-Gaussian fluctuations are present independently of topological transitions, the existence of a quantitative connexion between collective rearrangements and such transitions is still an open question (41). Our approach consists in reducing the dynamics of a large number of interacting vertices into the dynamics of a single vertex embedded in an effective background that describes the mean-field effect of the surrounding system. Within our model, interactions are embodied by both the elastic confinement and the active source of fluctuations leading to large

displacements. We argue below that our phenomenological approach is sufficient to capture the vertex dynamics, since it provides a framework to decipher the effects of the Rho pathway inhibitions on this dynamics.

Order relation in the active diffusion coefficient and the persistence time

We fit the MSD data with our analytic prediction to estimate the parameters characterizing nonequilibrium activity. Our fits convincingly capture the transition from sub-diffusive to super-diffusive like behaviors [Fig. 2(a)]. Within our model, these behaviors correspond to cross-over regimes between the short and large time diffusion. We extract from the best fits a single set of passive and active parameters for each condition. Our estimate for τ_c can be compared with

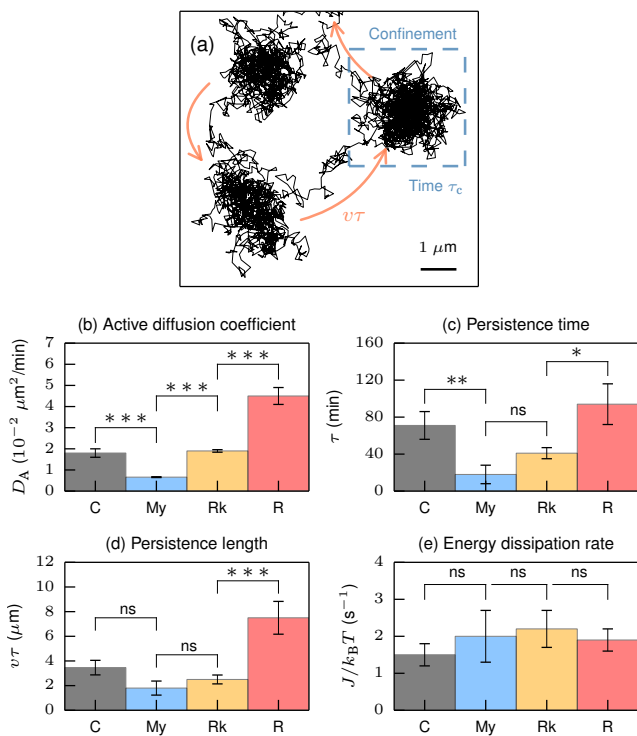


Figure 3: Active parameters of vertex fluctuations. (a) Typical trajectory obtained from simulations of the vertex dynamics in control condition (scale bar 1 μm). Isotropic “blobs” reveal equilibrium-like transient confinement during a typical time τ_c (dashed blue box), and large displacements of order $v\tau$ occur due to nonequilibrium activity (orange arrows). (b) Best fit values of the active diffusion coefficient, (c) the persistence time, (d) the persistence length, and (e) the energy dissipation rate. Statistical analysis with t-test: ns (non significant) $p > 0.05$, * $p < 0.05$, ** $p < 0.01$, *** $p < 0.001$ (see the Supporting Material).

timescales quantifying the transition from elastic to fluid-like behavior of the material (see Tab. S1 in the Supporting Material), which is of the same order as the Maxwell time reported in three-dimensional cell aggregates, *i.e.* about 30–40 min (9, 42–44). We report clear quantitative variations of both the active diffusion coefficient D_A and the persistence time τ for all conditions [Figs. 3(b,c)]. This suggests that our model, based on separating purely active fluctuations from equilibrium thermal ones, is a reliable framework to capture the effects of our inhibitors on tissue dynamics. Note that passive parameters, such as the relaxation time scale $\tau_r = \gamma/k$ reported in Tab. S1 (see the Supporting Material), have also different values between the conditions. This reflects the effects of inhibitors on tissue mechanics, showing that inhibitors also affects the characteristics of passive fluctuations. In this respect, D_A and τ are the parameters that characterize *only* the active contribution to vertex fluctuations, which is the main focus of our study.

Strikingly, D_A and τ are larger for Rho inhibitor than for Rho kinase inhibitor, and than for direct myosin inhibition [Figs. 3(b,c)]. The more upstream the inhibition along the pathway, the larger the amplitude of fluctuations and the more persistent the ensuing displacement. The myosin inhibition leads to the smallest D_A and τ values, suggesting that the mesoscopic activity of vertices is strongly affected. The Rho kinase target directly activates the myosin, but it also inhibits the myosin light chain phosphatase (MLCP) which in turn inhibits the myosin. Therefore, the result of Rho kinase inhibition on myosin can not be anticipated *a priori*. Our analysis shows that activity of vertices is less affected than for the myosin inhibitor case: the corresponding value of D_A for Rho kinase inhibitor is close to the one for control, which suggests a compensation between activation and de-activation of myosin.

Order relation confirmed by persistence lengths

To gain further insight into the active component of the dynamics, we compare the displacement PDF extracted from the simulated trajectories of vertex dynamics with experimental distributions. The distribution at short time is Gaussian and entirely controlled by the passive parameters: the simulations with or without active fluctuations, where we use passive parameters estimated from fits of MSD data, give the same results at short times (see yellow curves in Figs. 2(b-e)). Including the active component for the dynamics leaves us with one remaining free parameter: the average persistence length $v\tau$ of large displacements. The short time Gaussian remains unchanged, whereas exponential tails develop at large times in the simulated PDF. The tails are more pronounced as time increases, while the central Gaussian part barely changes. We adjust the $v\tau$ value by matching the tails appearing in numerical results and experimental data.

The simulated PDFs compare very well with experiments at large times, showing that our simulations reproduce the evolution of experimental distributions at all times [Figs. 2(b-e)]. This is one of the main success of our analysis: the phenomenological model on which relies the quantification of internal activity is able to capture the strong non-Gaussian tails of the distribution with only one free parameter. This supports the underlying picture that vertex dynamics essentially alternates between transient confinement and directed motions. The order of magnitude of the extracted mean persistence length $v\tau$ is consistent with our measurements [Fig. 3(d)]. We report again the same order relation within the Rho pathway, *i.e.* an increase of $v\tau$ from myosin inhibitor to Rho kinase inhibitor, and from Rho kinase inhibitor to Rho inhibitor, as a signature of enhanced directed motion.

Dissipation is constant for all inhibitors

A major asset of our model is that it allows us to predict the mean rate of energy dissipated by the vertex dynamics in its surrounding environment. It is defined as the difference between the power injected by the fluctuating thermal force and the one that the moving vertex dissipates *via* the drag force: $J = \langle \dot{x}(\gamma\dot{x} - \sqrt{2\gamma k_B T}\xi) \rangle$, where \dot{x} is the vertex velocity, and ξ is a zero-mean Gaussian white noise (45, 46). It vanishes for systems in a thermodynamic equilibrium state. The active nonequilibrium fluctuations lead to a non zero dissipation rate: $J = kD_A/(1 + \tau/\tau_r)$ (47). This rate of dissipated energy reflects the excess power injected by nonequilibrium internal activity driving the large displacements of vertices.

When computing the dissipation rate in the four conditions, it appears as approximately constant [Fig. 3(e)], in contrast with the order relation found for active parameters [Figs. 3(b-d)]. This supports that the same amount of energy is dissipated by the vertex large displacements, though the features of such displacements differ between conditions. Given that J depends both on parameters of active fluctuations $\{D_A, \tau\}$ and on parameters of passive mechanics $\{\gamma, k\}$, our result suggests that there may be an underlying coupling between mechanical properties of the tissue and its nonequilibrium fluctuations. A possible interpretation is that the nonequilibrium processes at the origin of active fluctuations, such as forces induced by myosin and by actin polymerization, might also affect the tissue mechanics in such a way that the dissipation rate remains unchanged over all the conditions. In that respect, we observe that the relaxation time τ_r is increased for Rho inhibitor case with respect to others (see Tab. S1 in the Supporting Material), as also observed for the persistence time τ [Fig. 3(c)].

DISCUSSION

The parameters of vertex fluctuations reveal a correlation between the Rho pathway hierarchy and the junction active fluctuations: the higher up the Rho pathway is the inhibition, the lower is the effect on decreasing the fluctuations of the vertices. Such a relation highlights the usefulness of our methodology to probe quantitatively how signaling pathways control emergent fluctuations. In that respect, our approach bridges biochemical signaling pathways with mechanical fluctuations *in vivo*. It could be used to characterize quantitatively the effect on fluctuations of other inhibitions acting on different signaling pathways.

Our analysis is based on a phenomenological model which deliberately avoids a detailed description of the many processes operating at the subcellular scale. It is also distinct from other models which consider explicit interactions between neighbouring cells. In that respect, our results do not rely neither on the microscopic details of activity-induced forces nor on the form of interactions within the tissue. We rather postulate an effective vertex dynamics by explicitly distinguishing thermal and active fluctuations. As a result, any underlying mechanism which could rationalize the relation between pathway inhibition and mechanical fluctuations is out of the scope of our approach. Yet, the relation between biochemical signaling and active fluctuations that we quantified in tissues could help future studies to understand the precise relation between the subcellular cytoskeleton dynamics and the emergent vertex fluctuations. In that respect, a possible extension of the model could consist in considering more complex activation/inhibition in the Rho pathway and their connection with contractile forces in the cell (17, 18).

In order to test the robustness of our model, one could measure the response of vertices to an external perturbation (48). The intracellular mechanics is viscoelastic in a large variety of living systems. Our phenomenological model has already been extended to account for a complex rheology (49). It would be interesting to determine whether the relation between fluctuations and pathway inhibitions is similar when including viscoelastic effects. Moreover, applying an external potential to confine a vertex, one could extract work from the vertex fluctuations by varying in time the potential parameters. Our framework allows one to predict the details of the extracted work as a function of the active fluctuation characteristics (47). Confronting such predictions with experimental results would provide another test for the validity of our approach.

The response in living systems is not related to the spontaneous fluctuations, in contrast to equilibrium where such a relation is given by the fluctuation-dissipation theorem (FDT). Therefore, by comparing the response with spontaneous fluctuations of tissues, one could quantify the departure from the FDT, namely the deviation of the dynamics

from equilibrium. Moreover, recent progress in nonequilibrium statistical mechanics have shed light on the direct relation between the rate of energy dissipated by the internal nonequilibrium processes and the violation of the FDT (50). This has already led to access to the dissipation rate in some biological contexts (49, 51). In that respect, comparing response and fluctuations will allow one to propose an alternative quantification of dissipation rates in epithelial tissues.

The Rho pathway is conserved across species, suggesting that regulations of activity in epithelial monolayers may share common pathways in a large variety of tissues and organisms (12). Our approach, based on a quantitative analysis of vertex fluctuations, could serve as a novel framework to decipher the complex regulation of spatial fluctuations by the Rho pathway in other model systems. In that respect, it could be used to analyze vertex fluctuations in developing embryos, such as in *Drosophila* or in *C. elegans*, where internal reorganizations are driven by spontaneous topological transitions (7, 8).

Author contributions

V.M., J.C., R.T., and D.R. designed and performed the experiments. É.F., N.S.G., P.V., and F.v.W. designed the model. All authors contributed to analyzing the data and writing the manuscript.

Acknowledgements

We thank F. Graner for helpful discussions. We acknowledge J. W. Nelson for sending the MDCK cell lines. We also thank N. Maggartou for extraction of data and lab. members for discussions. This work is supported by CNRS, FRC and University of Strasbourg. N.S.G. is the incumbent of the Lee and William Abramowitz Professorial Chair of Biophysics.

SUPPORTING MATERIAL

An online supplement to this article can be found by visiting BJ Online at <http://www.biophysj.org>.

References

1. Backouche, F., L. Haviv, D. Groswasser, and A. Bernheim-Groswasser, 2006. Active gels: dynamics of patterning and self-organization. *Physical Biology* 3:264.
2. Soares e Silva, M., B. Stuhmann, T. Betz, and G. H. Koenderink, 2014. Time-resolved microrheology of actively remodeling actomyosin networks. *New J. Phys.* 16:075010.
3. Blanchoin, L., R. Boujemaa-Paterski, C. Sykes, and J. Plastino, 2014. Actin dynamics, architecture, and mechanics in cell motility. *Physiological reviews* 94:235–263.
4. Murrell, M., P. W. Oakes, M. Lenz, and M. L. Gardel, 2015. Forcing cells into shape: the mechanics of actomyosin contractility. *Nature Reviews Molecular Cell Biology* 16:486–498.
5. Schuppler, M., F. C. Keber, M. Kröger, and A. R. Bausch, 2016. Boundaries steer the contraction of active gels. *Nature Communications* 7:13120.
6. Soares e Silva, M., M. Depken, B. Stuhmann, M. Korsten, F. C. MacKintosh, and G. H. Koenderink, 2011. Active multistage coarsening of actin networks driven by myosin motors. *Proc. Natl. Acad. Sci. USA* 108:9408–9413.
7. Rauzi, M., P. Verant, T. Lecuit, and P.-F. Lenne, 2008. Nature and anisotropy of cortical forces orienting *Drosophila* tissue morphogenesis. *Nature Cell Biology* 10:1401–1410.
8. Guillot, C., and T. Lecuit, 2013. Mechanics of Epithelial Tissue Homeostasis and Morphogenesis. *Science* 340:1185–1189.
9. Marmottant, P., A. Mgharbel, J. Käfer, B. Audren, J.-P. Rieu, J.-C. Vial, B. van der Sanden, A. F. M. Marée, F. Graner, and H. Delanoë-Ayari, 2009. The role of fluctuations and stress on the effective viscosity of cell aggregates. *Proc. Natl. Acad. Sci. USA* 106:17271–17275.
10. Cavey, M., M. Rauzi, P.-F. Lenne, and T. Lecuit, 2008. A two-tiered mechanism for stabilization and immobilization of E-cadherin. *Nature* 453:751–756.
11. Bardet, P.-L., B. Guirao, C. Paoletti, F. Serman, V. Lopold, F. Bosveld, Y. Goya, V. Mirouse, F. Graner, and Y. Bellaïche, 2013. PTEN Controls Junction Lengthening and Stability during Cell Rearrangement in Epithelial Tissue. *Developmental Cell* 25:534–546.
12. Etienne-Manneville, S., and A. Hall, 2002. Rho GTPases in cell biology. *Nature* 420:629–635.
13. Reyes, C., M. Jin, E. Breznau, R. Espino, R. Delgado-Gonzalo, A. Goryachev, and A. Miller, 2014. Anillin Regulates Cell-Cell Junction Integrity by Organizing Junctional Accumulation of Rho-GTP and Actomyosin. *Current Biology* 24:1263–1270.
14. Oakes, P. W., E. Wagner, C. A. Brand, D. Probst, M. Linke, U. S. Schwarz, M. Glotzer, and M. L. Gardel, 2016. Optogenetic control of RhoA reveals zyxin-mediated elasticity of stress fibres. *Nature Communications* 8:15817.
15. Gibson, M. C., A. B. Patel, R. Nagpal, and N. Perrimon, 2006. The emergence of geometric order in proliferating metazoan epithelia. *Nature* 442:1038–1041.
16. Riveline, D., E. Zamir, N. Q. Balaban, U. S. Schwarz, T. Ishizaki, S. Narumiya, Z. Kamb, B. Geiger, and A. D. Bershadsky, 2001. Focal Contacts as Mechanosensors. *J. Cell Biol.* 153:1175–1186.
17. Besser, A., and U. S. Schwarz, 2007. Coupling biochemistry and mechanics in cell adhesion: a model for inhomogeneous stress fiber contraction. *New J. Phys.* 9:425.
18. Bement, W. M., M. Leda, A. M. Moe, A. M. Kita, M. E. Larson, A. E. Golding, C. Pfeuti, K.-C. Su, A. L. Miller, A. B. Goryachev, and G. von Dassow, 2008. Activatorinhibitor coupling between Rho signalling and actin assembly makes the cell cortex an excitable medium. *Nature Cell Biology* 17:1471–1483.
19. Adams, C. L., Y. Chen, S. J. Smith, and W. J. Nelson, 1998. Mechanisms of Epithelial Cell-Cell Adhesion and Cell Compaction Revealed by High-resolution Tracking of E-Cadherin-Green Fluorescent Protein. *J. Cell Biol.* 142:1105–1119.

20. Salomon, J., C. Gaston, J. Magescas, B. D. D. Canioni, L. Sengmanivong, A. Mayeux, G. Michaux, F. Campeotto, J. Lemale, J. Viala, F. Poirier, N. Minc, J. Schmitz, N. Brousse, B. Ladoux, O. Goulet, and D. Delacour, 2017. Contractile forces at tricellular contacts modulate epithelial organization and monolayer integrity. *Nature Materials* 8.
21. Lye, C. M., H. W. Naylor, and B. Sanson, 2014. Subcellular localisations of the CPTI collection of YFP-tagged proteins in *Drosophila* embryos. *Development* 141:4006–4017.
22. Rauzi, M., P.-F. Lenne, and T. Lecuit, 2010. Planar polarized actomyosin contractile flows control epithelial junction remodelling. *Nature* 468:1110–1114.
23. Klingner, C., A. V. Cherian, J. Fels, P. M. Diesinger, R. Aufschnaiter, N. Maghelli, T. Keil, G. Beck, I. M. Tolić-Nørrelykke, M. Bathe, and R. Wedlich-Soldner, 2014. RhoA and RhoC have distinct roles in migration and invasion by acting through different targets. *J. Cell Biol.* 207:107–121.
24. Jin, Y., S. J. Atkinson, J. A. Marrs, and P. J. Gallagher, 2001. Myosin II Light Chain Phosphorylation Regulates Membrane Localization and Apoptotic Signaling of Tumor Necrosis Factor Receptor-1. *J. Biol. Chem.* 276:30342–30349.
25. Reffay, M., M. C. Parrini, O. Cochet-Escartin, B. Ladoux, A. Buguin, S. Coscoy, F. Amblard, J. Camonis, and P. Silberzan, 2014. Interplay of RhoA and mechanical forces in collective cell migration driven by leader cells. *Nature Cell Biology* 16:217–223.
26. Sorce, B., C. Escobedo, Y. Toyoda, M. P. Stewart, C. J. Cattin, R. Newton, I. Banerjee, A. Stettler, B. Roska, S. Eaton, A. A. Hyman, A. Hierlemann, and D. J. Müller, 2015. Mitotic cells contract actomyosin cortex and generate pressure to round against or escape epithelial confinement. *Nature Communications* 6:8872.
27. Imai, M., K. Furusawa, T. Mizutani, K. Kawabata, and H. Haga, 2015. Three-dimensional morphogenesis of MDCK cells induced by cellular contractile forces on a viscous substrate. *Scientific Reports* 5:14208.
28. Munjal, A., and T. Lecuit, 2014. Actomyosin networks and tissue morphogenesis. *Development* 141:1789–1793.
29. Wollrab, V., R. Thiagarajan, A. Wald, K. Kruse, and D. Riveline, 2016. Still and rotating myosin clusters determine cytokinetic ring constriction. *Nature Communications* 7:11860.
30. Nixon-Abell, J., C. J. Obara, A. V. Weigel, D. Li, W. R. Legant, C. S. Xu, H. A. Pasolli, K. Harvey, H. F. Hess, E. Betzig, C. Blackstone, and J. Lippincott-Schwartz, 2016. Increased spatiotemporal resolution reveals highly dynamic dense tubular matrices in the peripheral ER. *Science* 354.
31. Toyota, T., D. A. Head, C. F. Schmidt, and D. Mizuno, 2011. Non-Gaussian athermal fluctuations in active gels. *Soft Matter* 7:3234–3239.
32. Park, Y., C. A. Best, T. Auth, N. S. Gov, S. A. Safran, G. Popescu, S. Suresh, and M. S. Feld, 2010. Metabolic remodeling of the human red blood cell membrane. *Proc. Natl. Acad. Sci. USA* 107:1289–1294.
33. Ben-Isaac, E., Y. Park, G. Popescu, F. L. H. Brown, N. S. Gov, and Y. Shokef, 2011. Effective Temperature of Red-Blood-Cell Membrane Fluctuations. *Phys. Rev. Lett.* 106:238103.
34. Trepap, X., M. R. Wasserman, T. E. Angelini, E. Millet, D. A. Weitz, J. P. Butler, and J. J. Fredberg, 2009. Physical forces during collective cell migration. *Nature Physics* 5:426–430.
35. Bursac, P., G. Lenormand, B. Fabry, M. Oliver, D. Weitz, V. Viasnoff, J. Butler, and J. J. Fredberg, 2005. Cytoskeletal remodelling and slow dynamics in the living cell. *Nature Materials* 4:557–561.
36. Fodor, É., M. Guo, N. S. Gov, P. Visco, D. A. Weitz, and F. van Wijland, 2015. Activity-driven fluctuations in living cells. *EPL (Europhysics Letters)* 110:48005.
37. Farhadifar, R., J.-C. Roper, B. Aigouy, S. Eaton, and F. Jülicher, 2007. The Influence of Cell Mechanics, Cell-Cell Interactions, and Proliferation on Epithelial Packing. *Current Biology* 17:2095–2104.
38. Käfer, J., T. Hayashi, A. F. M. Marée, R. W. Carthew, and F. Graner, 2007. Cell adhesion and cortex contractility determine cell patterning in the *Drosophila* retina. *Proc. Natl. Acad. Sci. USA* 104:18549–18554.
39. Bi, D., J. H. Lopez, J. M. Schwarz, and M. L. Manning, 2015. A density-independent rigidity transition in biological tissues. *Nature Physics* 11:1074–1079.
40. Bi, D., X. Yang, M. C. Marchetti, and M. L. Manning, 2016. Motility-Driven Glass and Jamming Transitions in Biological Tissues. *Phys. Rev. X* 6:021011.
41. Bi, D., J. H. Lopez, J. M. Schwarz, and M. L. Manning, 2014. Energy barriers and cell migration in densely packed tissues. *Soft Matter* 10:1885–1890.
42. Forgacs, G., R. A. Foty, Y. Shafir, and M. S. Steinberg, 1998. Viscoelastic Properties of Living Embryonic Tissues: a Quantitative Study. *Biophys. J.* 74:2227–2234.
43. Guevorkian, K., M.-J. Colbert, M. Durth, S. Dufour, and F. Brochard-Wyart, 2010. Aspiration of Biological Viscoelastic Drops. *Phys. Rev. Lett.* 104:218101.
44. Stirbat, T. V., A. Mgharbel, S. Bodenec, K. Ferri, H. C. Meriani, J.-P. Rieu, and H. Delanoë-Ayari, 2013. Fine Tuning of Tissues' Viscosity and Surface Tension through Contractility Suggests a New Role for α -Catenin. *PLoS ONE* 8:e52554.
45. Sekimoto, K., and S. Sasa, 1997. Complementarity Relation for Irreversible Process Derived from Stochastic Energetics. *J. Phys. Soc. Jpn.* 66:3326–3328.
46. Sekimoto, K., 1997. Kinetic Characterization of Heat Bath and the Energetics of Thermal Ratchet Models. *J. Phys. Soc. Jpn.* 66:1234–1237.
47. Fodor, É., K. Kanazawa, H. Hayakawa, P. Visco, and F. van Wijland, 2014. Energetics of active fluctuations in living cells. *Phys. Rev. E* 90:042724.
48. Harris, A. R., L. Peter, J. Bellis, B. Baum, A. J. Kabla, and G. T. Charras, 2012. Characterizing the mechanics of cultured cell monolayers. *Proc. Natl. Acad. Sci. USA* 109:16449–16454.
49. Fodor, É., W. W. Ahmed, M. Almonacid, M. Bussonnier, N. S. Gov, M.-H. Verlhac, T. Betz, P. Visco, and F. van Wijland, 2016. Nonequilibrium dissipation in living oocytes. *EPL (Europhysics Letters)* 116:30008.
50. Harada, T., and S.-i. Sasa, 2005. Equality Connecting Energy Dissipation with a Violation of the Fluctuation-Response Relation. *Phys. Rev. Lett.* 95:130602.
51. Toyabe, S., T. Okamoto, T. Watanabe-Nakayama, H. Takekuni, S. Kudo, and E. Muneyuki, 2010. Nonequilibrium Energetics of a Single F1-ATPase Molecule. *Phys. Rev. Lett.* 104:198103.